

B-spline velocity field level set topology optimization method for stress and buckling constraints based on discrete adjoint method

Hao Deng*, and Kazuhiro Saitou

Department of Mechanical Engineering, University of Michigan, Ann Arbor, MI 48109

*Corresponding author. Email: denghao@umich.edu

Abstract

This paper proposes a new sensitivity computational scheme for velocity field level set method with discrete adjoint method. The velocity field of level set method is described in B-spline space. The adjoint equations are constructed based on discretized governing equations. This paper demonstrates that the velocity field of level set method can be fully derived from the discrete adjoint method. This enables the circumvention of shape sensitivity analysis for standard level set method. We demonstrate the effectiveness of proposed method in the context of stress and linearized buckling topology optimization problems.

Keywords: Topology optimization, discrete adjoint sensitivities, level set method, stress constraints, buckling constraints.

1. Introduction

Topology optimization has become an important tool to determine the optimal shape for maximum performance subject to given design constraints. After three decades of development, several topology optimization methods have been proposed and gained popularity, such as, density-based method [1], level set method [2], and BESO method [3]. Besides, other new methods have also been developed in recent years such as moving morphable components (MMC) [4-6], moving morphable voids (MMV) [7], and geometry projection method [8-10].

The Level set method (LSM) is one of the popular methods used for topology and shape optimization. For standard level set method, the topology of structure is described implicitly using the level set function ϕ , where the boundary is determined by $\{\phi = 0\}$. In classical LSM, the boundary is updated through evolving the implicit function ϕ based on Hamilton-Jacobi equation. In general, the optimization problem needs to be transformed in an unconstrained problem, where the lagrangian formulations are applied to deal with constraints. For classical LSM, the lagrangian multipliers are gradually updated based on a certain strategy to avoid fluctuations and ensure convergence. The evolution of implicit level set function is driven by normal boundary velocity in the design domain based on natural velocity extension [11] or the fast-marching method [12]. Besides classic LSM, the parametric level-set method has drawn great attention in recent years. Wang et al [13] proposed an RBF-level set optimization method to transform the Hamilton-Jacobi equation into a system of ordinary differential equations (ODEs) based on collocation formulation. Since then, several parametric level-set methods [14-16] with different basis functions for various physical problems have been developed. Recently, a velocity field level-set (VFLS) method [17, 18] is proposed by Wang et al. The key point of VFLS method is construct the boundary normal velocity field in the design domain, which is used to update the level set function. Note that the velocity field is controlled by prescribed basis functions and velocity design variables at given points. VFLS method provides an effective way to

handling multiple constraints, and standard mathematical programming algorithm can be incorporated. Furthermore, Wang et al [19] incorporates the topological derivative concept into velocity field level set method to enable automatic nucleation of interior holes. A comprehensive literature review for level set methods in topology optimization can be found in Ref [20].

For classical level set topology optimization method, the continuous adjoint method is widely used to compute sensitivities [11]. One of the major obstacles of continuous adjoint method is the sensitivity expressions are discontinuous at nodes and edges of finite elements. In general, interpolation and smoothing techniques are needed to avoid discontinuity, which inevitable results in a reduction of sensitivity accuracy. This sensitivity processing method may lead to diverge for high move limits as demonstrated by Sandilya and Alicia et al [21]. As pointed by Alicia et al, the classical continuous adjoint method follows the differentiate-then-discretize scheme [22]. Compared to the classical continuous adjoint method, the discrete adjoint method follows a different discretize-then-differentiate philosophy. As described in Ref [21], the discrete adjoint method discretizes the partial differential equations using finite element method first. The discretized equations are then differentiated to obtain adjoint equations based on augmented functional equations. The discretize adjoint method is widely used in density-based topology optimization method [23] for sensitivity derivation, while Sandilya and Alicia et al [21] introduced the discrete adjoint method into classical level set method for the first time using a semi-analytical formulation. Compare to the semi-analytical formulation, where the boundary is perturbed implicitly to obtain level set sensitivity (or velocity) based on finite difference approximation, an analytical formulation method is proposed in this paper to bridge the gap between the discrete adjoint sensitivity with classical level set sensitivity in the framework of velocity field level set method. In the proposed method, the normal boundary velocity of level set method can be readily derived from discrete adjoint method. The major contribution of this paper comes from three aspects 1) the analytical formulation linking discrete adjoint method with level set boundary velocity is derived and demonstrated from mathematical perspective. 2) B-spline basis is introduced into velocity field level set method. 3) The stress and local buckling constraints are considered for volume minimization problem in the framework of level set topology optimization method.

The remainder of the paper is organized as follows. Section 2 presents the mathematical formulation of B-spline velocity field level set method based on discrete adjoint method. Section 3 demonstrates two typical topology optimization problems with local stress and buckling constraints to verify the effectiveness of the proposed method, followed by conclusions in Section 4.

2. B-spline Velocity Field Level Set Topology Optimization Method

2.1 B-spline velocity field level set method

For level set method, the material domain Ω in an initial design domain D can be represented by an implicit level-set function as follows,

$$\begin{cases} \Phi(x) > 0 & x \in \Omega \setminus \partial\Omega \\ \Phi(x) = 0 & x \in \partial\Omega \cap D \\ \Phi(x) < 0 & x \in D \setminus \Omega \end{cases} \quad (1)$$

where $\Phi(x)$ is signed distance function. The shape and topology of material domain evolves through boundary moving, which is achieved through the Hamilton-Jacobi equation based on a given normal velocity V^n as follows,

$$\frac{\partial \Phi}{\partial t} - V^n |\nabla \Phi| = 0 \quad (2)$$

Here, the normal velocity field $V^n(\mathbf{x}, t)$ (two dimension) is constructed using B-spline basis functions and velocity design variables $b_{k,l}$ as following,

$$V^n(\mathbf{x}, y, t) = \sum_{k=0}^n \sum_{l=0}^m B_{k,p}(\mathbf{x}) B_{l,q}(y) b_{k,l} \quad (3)$$

Note that $\{B_{k,p}\}$ and $\{B_{l,q}\}$ are B-spline basis functions determined by knot vectors in x and y directions. p and q are the degrees of the B-spline basis functions. $B_{k,l}$ is the $(n+1) \times (m+1)$ B-spline coefficient. B-splines are commonly used in data interpolation and computer-aided design (CAD) [24]. In general, a degree p B-spline basis function $\{B_{k,p}\}$ is defined by a knot vector $\chi = \{\bar{x}_0, \bar{x}_1, \dots, \bar{x}_{n+p+1}\}$. Note that knot vector χ is a set of non-decreasing real numbers in design space, and interval $[\bar{x}_i, \bar{x}_{i+1}]$ is the i th knot span. In this paper, a uniform B-splines are used, where the knots are uniformly spaced in the parametric design space. The i th ($i=0, 1, \dots, n$) B-spline basis function can be defined in a recursion way as follows,

$$B_{i,p}(\mathbf{x}) = \frac{(x - \bar{x}_i) B_{i,p-1}(\mathbf{x})}{\bar{x}_{i+p} - \bar{x}_i} + \frac{(\bar{x}_{i+p+1} - x) B_{i+1,p-1}(\mathbf{x})}{\bar{x}_{i+p+1} - \bar{x}_{i+1}} \quad (4)$$

$$B_{i,0}(\mathbf{x}) = \begin{cases} 1 & \bar{x}_i \leq x \leq \bar{x}_{i+1} \\ 0 & \text{otherwise} \end{cases}$$

It is worth to mention that B-spline basis function is local support and non-negative, and B-spline basis should satisfy,

$$\sum_{i=0}^n B_{i,p}(\mathbf{x}) = 1 \quad (5)$$

More details regarding B-spline properties and theory can be found in Ref [25]. Once the velocity field is obtained, the level set function can be updated through Eq. (2) using the upwind difference scheme [12] and the method of moving asymptotes (MMA) algorithm [26]. Then, the re-initialization step is implemented to avoid numerical deterioration of the level set function. More implementation details can be found in Ref [17].

2.2 Sensitivity analysis based on discrete adjoint method

In this section, we present a discrete adjoint method for computing the velocity field in the design domain, which is used to update the level set equation in Eq. (2). For standard density-based method in the framework of the SIMP (Solid isotropic material with penalization) [1], the general sensitivity derivation based on the discrete adjoint method [27] is described in this section. The discretized governing equation for linear elastic problem can be written as follows,

$$\boldsymbol{\Psi} = \mathbf{K}\mathbf{u} - \mathbf{f} = \mathbf{0} \quad (6)$$

where \mathbf{K} is the stiffness matrix, \mathbf{u} is the displacement vector, and \mathbf{f} is the nodal force vector. Note that any other constraint equations for physical problems are written as follows,

$$\mathcal{H} = \mathbf{0} \quad (7)$$

For a given objective or constraint function F , an augmented Lagrangian function is formulated based on the adjoint method as follows,

$$G = F + \boldsymbol{\psi}^T \boldsymbol{\Psi} + \boldsymbol{\kappa}^T \mathcal{H} \quad (8)$$

where $\boldsymbol{\psi}$ and $\boldsymbol{\kappa}$ are Lagrange multiplier. Based on the discrete adjoint method, the sensitivity of augmented Lagrangian function G with respect to density ρ can be expressed as follows,

$$\frac{\partial G}{\partial \rho} = \frac{\partial F}{\partial \rho} + \boldsymbol{\psi}^T \frac{\partial \boldsymbol{\Psi}}{\partial \rho} + \boldsymbol{\kappa}^T \frac{\partial \mathcal{H}}{\partial \rho} \quad (9)$$

where Lagrange multiplier should satisfy,

$$\boldsymbol{\psi}^T \frac{\partial \boldsymbol{\Psi}}{\partial U} + \boldsymbol{\kappa}^T \frac{\partial \mathcal{H}}{\partial U} + \frac{\partial F}{\partial U} = \mathbf{0} \quad (10)$$

The above generalized derivation is usually referred to as the discrete adjoint method. In the rest of this section, we will derive the sensitivity of the function F with respect to the velocity field V^n of level set. Based on the chain rule,

$$\frac{\partial F}{\partial V_j^n} = \sum_{i=1}^{nele} \frac{\partial F}{\partial \rho_i} \frac{\partial \rho_i}{\partial V_j^n} \quad (11)$$

where the first term $\frac{\partial F}{\partial \rho_i}$ can be obtained through Eq. (9), and V_j^n is the velocity at j th velocity point. The second term $\frac{\partial \rho_i}{\partial V_j^n}$ corresponds to the change in the volume fraction (density) of the i th element due to the j th point velocity variation. $nele$ denotes number of finite elements. Note that Kambampati et al [21] apply perturbation of the boundary implicitly nearby the boundary point to approximate the second term $\left(\frac{\partial \rho_i}{\partial V_j^n}\right)$ with finite difference method. In this paper, the analytical derivation is proposed and formulated for the term $\left(\frac{\partial \rho_i}{\partial V_j^n}\right)$ as follows,

$$\frac{\partial \rho_i}{\partial V_j^n} = \frac{\partial H(\Phi_i)}{\partial V_j^n} = \delta(\Phi_i) \cdot \frac{\partial \Phi_i}{\partial V_j^n} \quad (12)$$

where $H(\cdot)$ is Heaviside function, and $\delta(\cdot)$ is Dirac function. These two functions can be approximated by [2],

$$H(x) = \begin{cases} \frac{3(1-\alpha)}{4} \left(\frac{x}{\Delta} - \frac{x^3}{3\Delta^3} \right) + \frac{1+\alpha}{2} & x < -\Delta \\ 1 & -\Delta \leq x < \Delta \\ \frac{3(1-\alpha)}{4\Delta} \left(1 - \frac{x^2}{\Delta^2} \right) & x \geq \Delta \end{cases} \quad (13)$$

$$\delta(x) = \begin{cases} 0 & |x| > \Delta \\ 1 & |x| \leq \Delta \end{cases} \quad (14)$$

where α is a small positive number ($\alpha = 1 \times 10^{-4}$), and 2Δ describe the width of the smooth region ($\Delta = 0.5$). Equation (2) can be rewritten as following forms,

$$d\Phi_i - V_i^n |\nabla \Phi_i| dt = 0 \quad (i = 1, 2, \dots, N) \quad (15)$$

where dt is a pseudo time, Φ_i is short for $\Phi(\mathbf{x}_i)$, and V_i^n denotes $V_n(\mathbf{x}_i)$. N is number of velocity points. We assume a small perturbation δV_i^n of velocity V_i^n , and corresponding variation of $d\Phi_i$ is $\delta \Phi_i$. Thus,

$$(d\Phi_i + \delta \Phi_i) - (V_i^n + \delta V_i^n) |\nabla \Phi_i| dt = 0 \quad (16)$$

Note that in above equation the effect of small perturbation $\delta \Phi_i$ on term $|\nabla \Phi_i|$ is ignored. Above equation can be simplified as,

$$\delta \Phi_i - \delta V_i^n |\nabla \Phi_i| dt = 0 \quad (17)$$

Therefore,

$$\frac{\partial \Phi_i}{\partial V_i^n} = |\nabla \Phi_i| dt \quad (18)$$

Note that the pseudo time dt here can be assumed to be 1, because the dt is just a scaling factor of sensitivity $\frac{\partial F}{\partial V_j^n}$, which will not have any effect on optimization progress if the method of moving asymptotes (MMA) [26] solver is applied to update the level set function, because the MMA optimizer is able to automatically tune the moving steps in optimization. To obtain the sensitivity of function F with respect to velocity design variables $b_{k,l}$ according to Eq. (3), we have,

$$\frac{\partial \rho_i}{\partial b_{k,l}} = \delta(\Phi_i) \cdot \sum_{j=1}^N \frac{\partial \Phi_i}{\partial V_j^n} \cdot \frac{\partial V_j^n}{\partial b_{k,l}} = \delta(\Phi_i) \cdot \sum_{j=1}^N \left(\delta_{ij} \frac{\partial \Phi_i}{\partial V_j^n} \cdot B_{k,p}(x_j) B_{l,q}(y_j) \right) \quad (19)$$

Note that $\delta_{ij} = 1$ if $i = j$, otherwise $\delta_{ij} = 0$. Thus,

$$\frac{\partial \rho_i}{\partial b_{k,l}} = \delta(\Phi_i) |\nabla \Phi_i| B_{k,p}(x_i) B_{l,q}(y_i) \quad (20)$$

Note that (x_i, y_i) is the coordinate of centroid of the i th element. Therefore, according to the Eq. (11), the sensitivity of function F with respect to velocity design variable $b_{k,l}$ can be given as,

$$\frac{\partial F}{\partial b_{k,l}} = \sum_{i=1}^{nele} \left(\frac{\partial F}{\partial \rho_i} \delta(\Phi_i) |\nabla \Phi_i| B_{k,p}(x_i) B_{l,q}(y_i) \right) \quad (21)$$

Based on the above equation, the sensitivity of target function F with respect to velocity design variable $b_{k,l}$ can be readily inherit from the discrete adjoint sensitivity $\frac{\partial F}{\partial \rho_i}$ using the chain rule. The formulation in Eq. (21) effectively unified the discrete adjoint sensitivity and level set velocity field.

3. Stress and Buckling Constrained Topology Optimization

3.1 Sensitivity analysis of stress constraint problem based on discrete adjoint method

For standard density-based method, the discretized linear elastic equations can be written as,

$$\mathbf{K}\mathbf{u} = \mathbf{f} \quad (22)$$

where \mathbf{K} is the global stiffness matrix, \mathbf{u} is displacement vector, and \mathbf{f} is force vector. The global stiffness matrix can be assembled by elemental stiffness matrix $\mathbf{K}_{e,i}$ as follows,

$$\mathbf{K} = \sum_i^N \mathbf{K}_{e,i} \quad (23)$$

where i denotes the i th element stiffness matrix. The element stiffness matrix using Ersatz material can be written as

$$\mathbf{K}_{e,i} = (E_{min} + \rho_i(E - E_{min})) \mathbf{K}_0 \quad (24)$$

where ρ_i is the density (volume fraction) of the i th element. E_{min} is the elasticity modulus of a void element, which is a small value to avoid numerical issue. \mathbf{K}_0 is the stiffness matrix for unit elasticity modulus. The maximum von-mises stress can be approximated by p-norm stress [28], which can be written as,

$$\sigma_p = \left(\sum_i^N \sigma_{vm,i}^p \right)^{1/p} \quad (25)$$

where $\sigma_{vm,i}$ is the von Mises stress of the i th element. N is the total number of elements. As described in Section 2.2, the augmented Lagrangian function \mathcal{L}_p can be formulated as follows,

$$\mathcal{L}_p = \sigma_p + \boldsymbol{\lambda}_p^T (\mathbf{K}\mathbf{u} - \mathbf{f}) \quad (26)$$

The adjoint vector $\boldsymbol{\lambda}_p$ can be obtained through solving $\frac{\partial \mathcal{L}_p}{\partial \mathbf{u}} = 0$. Therefore, the sensitivity of p-norm stress with respect to elemental density is given by,

$$\frac{\partial \mathcal{L}_p}{\partial \rho_i} = \frac{\partial \sigma_p}{\partial \rho_i} + \boldsymbol{\lambda}_p^T \frac{\partial \mathbf{K}}{\partial \rho_i} \mathbf{u} \quad (27)$$

The detailed derivation of p-norm stress sensitivity can be found in Ref [29].

3.2 Sensitivity analysis of buckling constraint problem based on discrete adjoint method

In this section, the sensitivity of fundamental buckling load factor (BLF) with respect to elemental density is derived. Similarly, the elemental stiffness matrix can be represented by Ersatz material model as shown in Eq. (24). The fundamental buckling load factor λ_f can be formulated as Rayleigh quotient [30],

$$\lambda_f(\boldsymbol{\rho}, \mathbf{u}) = \min \left(-\frac{\mathbf{v}^T \mathbf{K}[\boldsymbol{\rho}] \mathbf{v}}{\mathbf{v}^T \mathbf{G}[\boldsymbol{\rho}, \mathbf{u}] \mathbf{v}} \right) \quad (\mathbf{v} \in \mathbb{R}^n, \mathbf{v} \neq \mathbf{0}) \quad (28)$$

where \mathbf{G} is the global stress stiffness matrix, \mathbf{u} is the displacement vector. \mathbf{K} is the linear stiffness matrix. The general procedure of linearized buckling analysis is as follows, a) Define a reference load vector \mathbf{f} b) Compute the equilibrium displacement $\mathbf{u} = \mathbf{K}[\boldsymbol{\rho}]^{-1} \mathbf{f}$ c) Set up the stress stiffness matrix $\mathbf{G}[\mathbf{x}, \mathbf{u}(\mathbf{x})]$ d) compute the buckling load and corresponding buckling mode ($\lambda_i, \boldsymbol{\varphi}_i$) using the following equations,

$$(\mathbf{K}(\boldsymbol{\rho}) + \lambda \mathbf{G}[\boldsymbol{\rho}, \mathbf{u}(\boldsymbol{\rho})]) \boldsymbol{\varphi} = \mathbf{0}, \quad \boldsymbol{\varphi} \neq \mathbf{0} \quad (29)$$

The buckling modes are normalized such that $\boldsymbol{\varphi}_i^T \mathbf{K}[\boldsymbol{\rho}] \boldsymbol{\varphi}_j = \delta_{ij}$. Note that the sensitivity of the i th eigenvalue λ_i with respect to elemental density ρ_e is expressed as [31],

$$\frac{\partial \lambda}{\partial \rho_e} = \boldsymbol{\varphi}_i^T \left(\frac{\partial \mathbf{K}}{\partial \rho_e} + \lambda_i \frac{\partial \mathbf{G}}{\partial \rho_e} \right) \boldsymbol{\varphi}_i - \lambda_i \mathbf{z}_i^T \frac{\partial \mathbf{K}}{\partial \rho_e} \mathbf{u} \quad (30)$$

where \mathbf{z}_i can be obtained through solving adjoint equations,

$$\mathbf{K} \mathbf{z}_i = \boldsymbol{\varphi}_i^T (\nabla_{\mathbf{u}} \mathbf{G}) \boldsymbol{\varphi}_i \quad (31)$$

For local buckling constraint, an aggregation function is applied to generate a single constraint. Here, the KS function [32] is implemented as follow,

$$KS[\mu_i] = \mu_1 + \frac{1}{\gamma} \ln \left(\sum_{i=1}^q e^{\gamma(\mu_i - \mu_1)} \right) \quad (i \in \mathbb{Z}) \quad (32)$$

Note that $\mu_i = 1/\lambda_i$, where the degree of smoothness is governed by the aggregation parameter γ . \mathbb{Z} is the set of interested μ_i . The value obtained by KS function produce an upper bound of $\max_{i \in \mathbb{Z}} |\mu_i|$. The range of parameter γ should be $[1, \infty)$. The first order derivative of KS function $KS[\mu_i]$ with respect to density ρ_e can be written as,

$$\frac{\partial KS[\mu_i]}{\partial \rho_e} = \frac{\sum_{i=1}^q \left(e^{\gamma(\mu_i - \mu_1)} \frac{\partial \mu_i}{\partial \rho_e} \right)}{\sum_{i=1}^q e^{\gamma(\mu_i - \mu_1)}} \quad (33)$$

The detailed sensitivity derivation and implementation can be found in Ref. [30].

3.3 Topology Optimization Problem Formulation

In this section, the optimization problem is volume minimization subject to stress and local buckling constraint. The optimization problem can be formulated as,

$$\begin{aligned} & \min V \\ & \text{s.t. } \sigma^{PM} \leq \sigma^* \\ & \text{s.t. } KS[\mu_i]_{(i \in \mathbb{Z})} \leq \mu^* \end{aligned} \quad (34)$$

In above formulation, the σ^{PM} denotes the p-norm stress, and σ^* is the upper limit of σ^{PM} . The upper bound of KS aggregation function $KS[\mu_i]_{(i \in \mathbb{Z})}$ is set to be μ^* . It is worth to mention that the parameters p and γ are selected as $p = 8, \gamma = 50$ in this paper. Note that the sensitivities of σ^{PM} and $KS[\mu_i]_{(i \in \mathbb{Z})}$ with respect to B-spline coefficients of velocity field are readily to be derived based on the mathematical formulation in Eq. (33), Eq. (27) and Eq. (21).

4. Numerical Examples

4.1 Compressed cube design

4.1.1 Volume minimization with p-norm stress constraint

The first example considers a compressed cube design, as illustrated in Fig. 1. The load is uniformly distributed at the middle of the top surface and has total magnitude $|F| = 1$. The cube is discretized by 300×300 finite elements with unit element length. The elastic modulus of the material is $E = 1$, and Poisson's ratio is chosen as $\nu = 0.3$. The bounds of the velocity design variables are selected as ± 0.2 , and the moving limit of MMA algorithm is 0.2. The B-spline knots are uniformly distributed in the design domain with a fixed interval Δ as shown in Fig. 1. The initialization of level set function is plotted in Fig. 2. In this section, the objective is minimizing the volume fraction with the p-norm stress constraint. The upper bound of p-norm stress σ^* is set to be $\sigma^* = 1.3$. In this simple example, we will examine the effect of knot number on optimal topology design. Three different B-spline knot span lengths Δ are applied, and corresponding optimized structures are demonstrated in Fig. 3-5. Note that we assume that the length of cube is L . The lowest volume fraction ($V = 0.075$) is reached if $\Delta = 0.1L$. Compared to the larger value of knot span length ($\Delta = 0.04$), small Δ means more design freedoms are achieved.

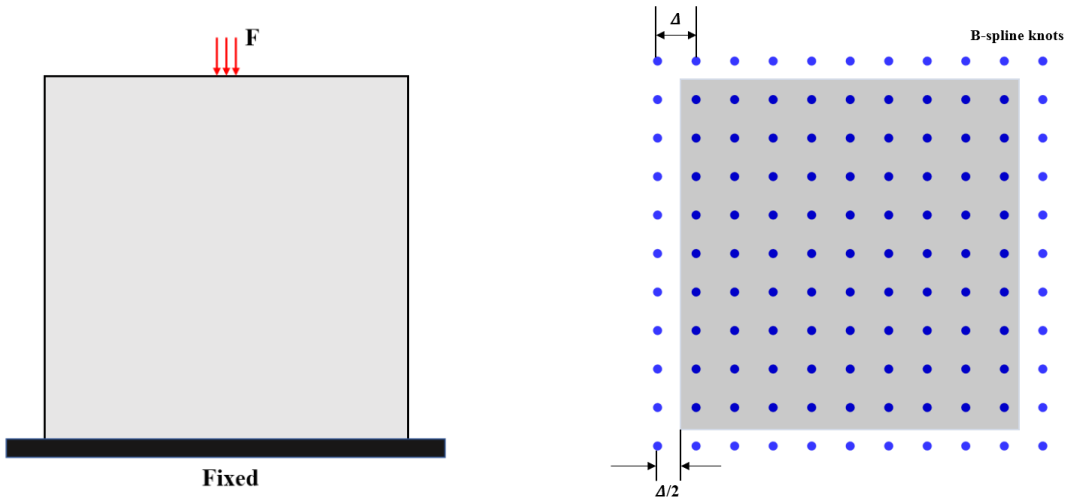


Figure 1. Compressed cube design

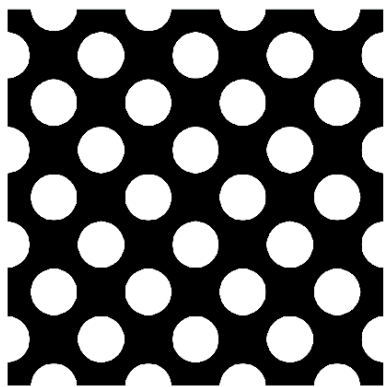
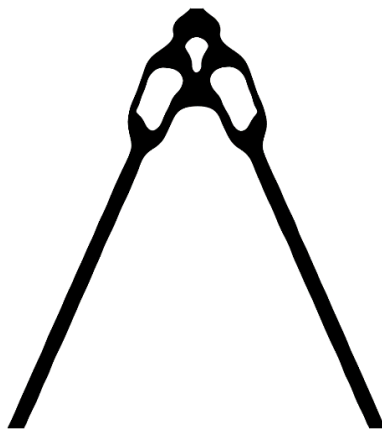


Figure 2. Level set initialization

(a) material layout



(b) von Mises stress distribution

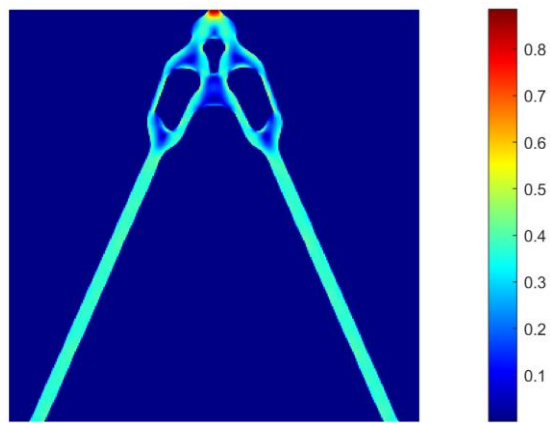


Figure 3. Optimized result (a) material layout (b) von Mises stress distribution ($V = 0.09, \Delta = 0.04$)

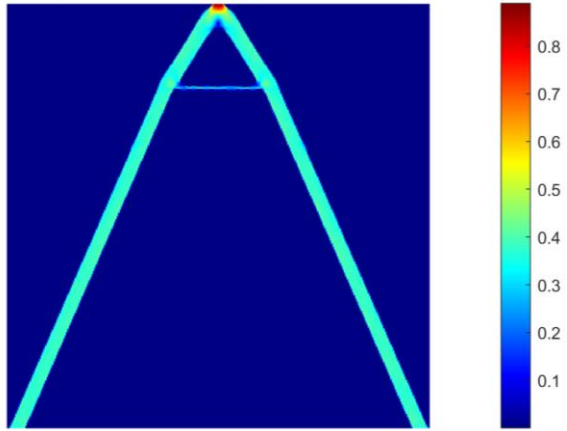
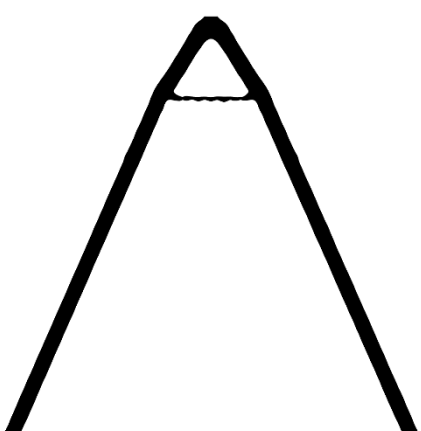


Figure 4. Optimized result (a) material layout (b) von Mises stress distribution ($V=0.078, \Delta=0.02$)

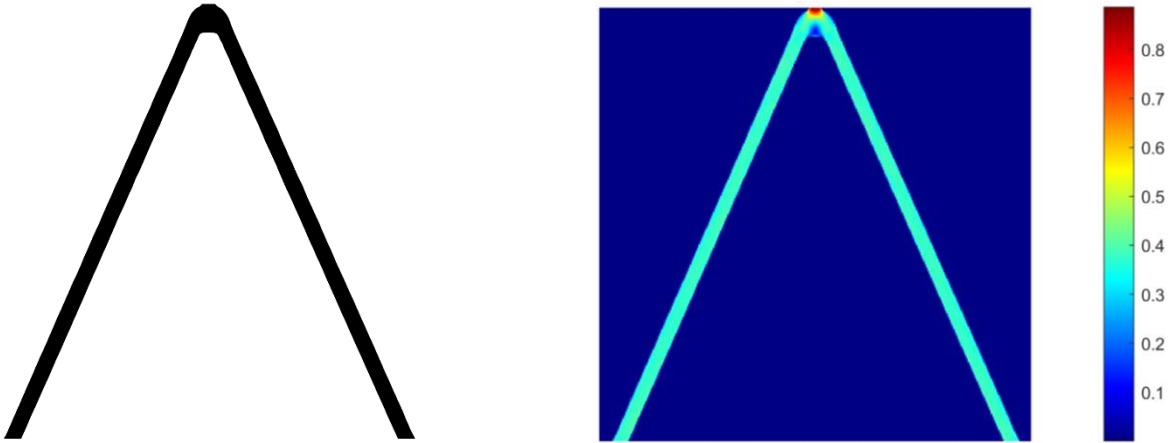


Figure 5. Optimized result (a) material layout (b) von Mises stress distribution ($V = 0.075, \Delta=0.01$)

4.1.2 Volume minimization with buckling constraint

In this section, the objective is minimizing the volume fraction with fundamental buckling load constraint. The force is uniform distributed on the four nodes at the mid of the upper edge. The total force magnitude is $|F| = 10^{-3}$. The buckling constraint μ^* is set to be $\mu^* = 0.15$. The finite element discretization, optimization setting, and material properties are the same as section 4.1.1. The B-spline knot span length is chosen as $\Delta=0.01$. The optimization progress converges once the relative difference of the target function between two adjacent iterations is smaller than 10^{-4} . The initial design and optimized design are demonstrated in Fig. 6. The objective function value decreases steadily until convergence is achieved. Because the fundamental buckling load need to compute through solving eigenvalue problem, which is highly sensitivity to boundary movement, some local small fluctuations are found in optimization. The volume fraction of designs decreases from 0.61 to 0.201 after 500 iterations.

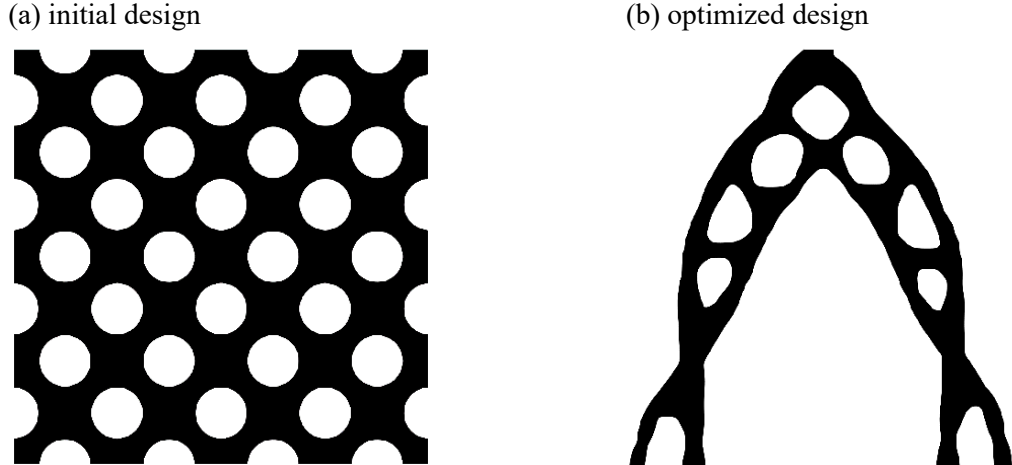


Figure 6. (a) initial design (b) optimized design

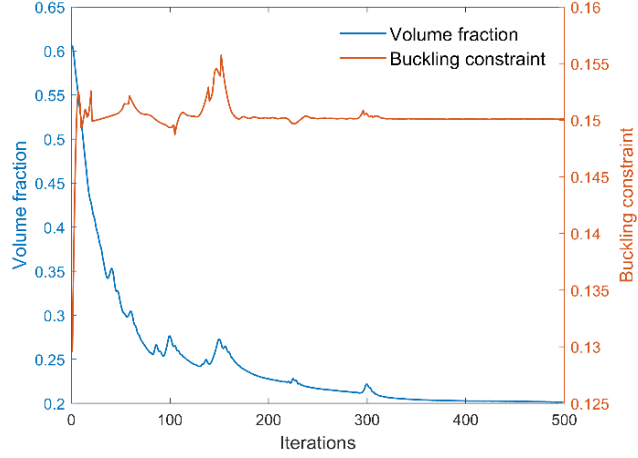


Figure 7. Convergence history of buckling constraint design

4.1.3 Volume minimization with buckling and stress constraint

This example applies volume minimization with stress and buckling load constraints. Similar to the previous numerical examples, the constraint for p-norm stress σ^* and buckling constraint μ^* are set to be $\sigma^* = 1.3$ and $\mu^* = 0.15$. Correspondingly, the loading force on the mid upper surface for stress and buckling are the same as section 4.1.1 and 4.1.2, separately. Other optimization configurations are the same as previous examples. The optimized design is plotted in Fig. 8(a), where the von Mises distribution is shown in Fig. 8(b). Fig. 9 presents the evolution of material layout. Due to the buckling load constraint, no slender beam structures are found in final design. The convergence history is demonstrated in Fig. 10. The volume fraction decreases steadily from initial value nearby 0.6 to 0.216 after optimization.

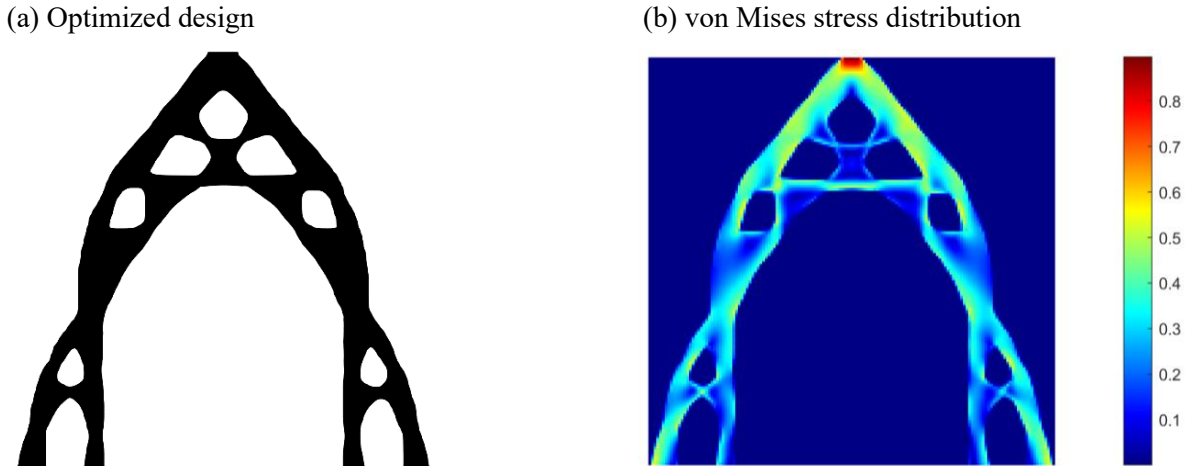


Figure 8. (a) Optimized design (b) von Mises stress distribution

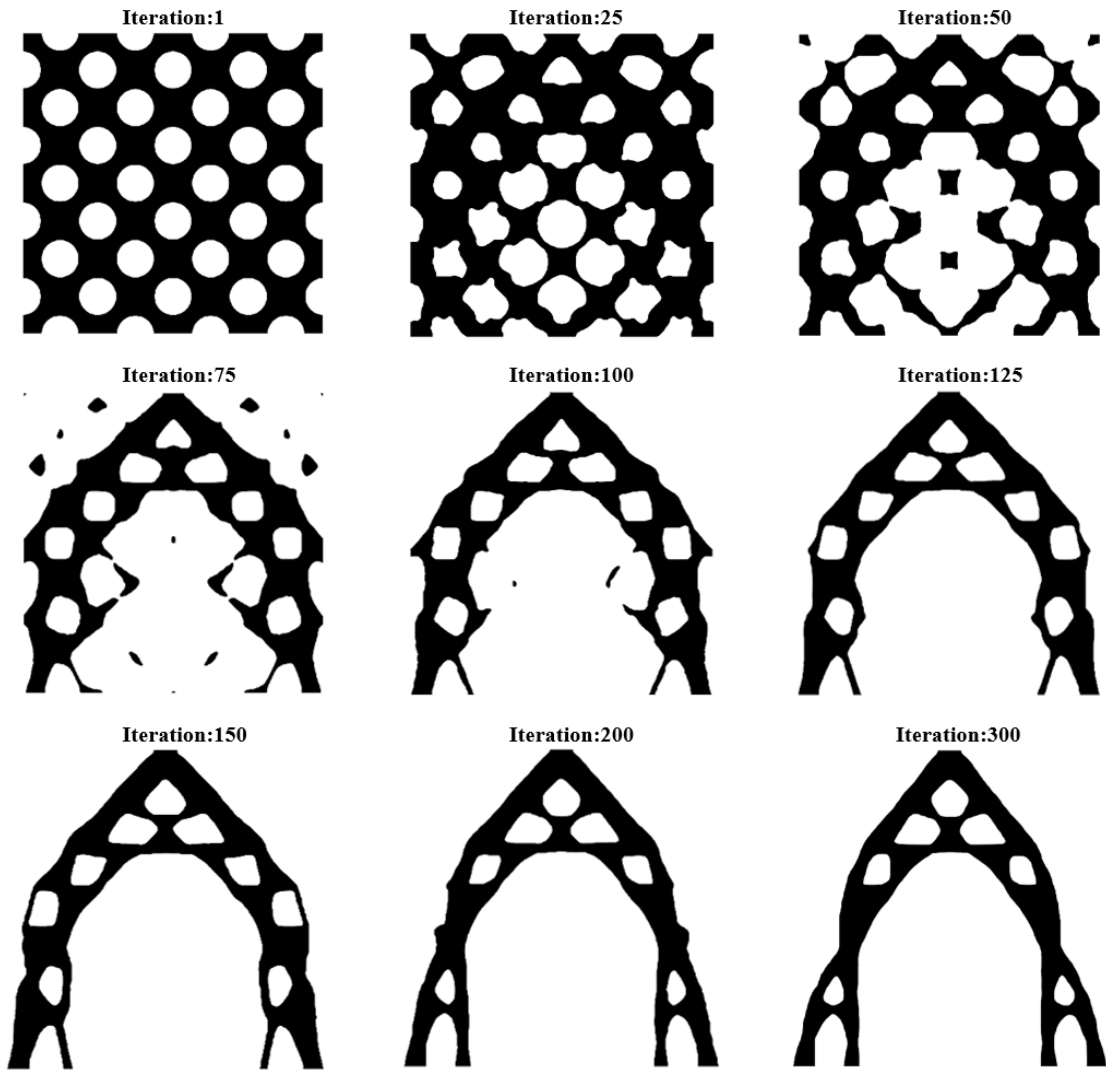


Figure 9. Evolution of material layout

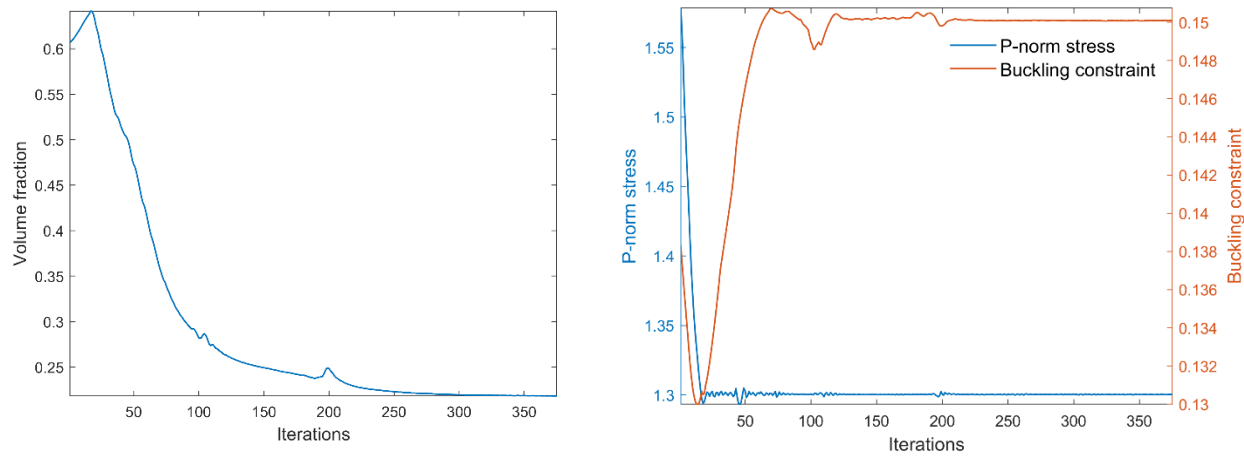


Figure 10. Convergence history

4.2 L-bracket design

4.2.1 volume minimization with stress constraint

Herein volume minimization of the L-bracket model presented in Fig. 11 is explored. The dimension of L-bracket is demonstrated in Fig. 11. Note that the domain is discretized by 100×100 finite element mesh, where a 60×60 section is removed to create L-bracket domain. A vertical load $F_p = 1$ is applied on the right upper corner for stress constraint problem. For this case, the elastic modulus and Poisson's ratio are selected as: $E = 1$, $\mu = 0.3$. The B-spline velocity knots are uniformly distributed in the whole design domain as shown in Fig. 11. Assuming that the maximum length of L-bracket is L , the value of knot interval Δ is selected as $\Delta = 0.02L$. Similarly, the bounds of the velocity design variables are selected as ± 0.2 , and the moving limit of MMA algorithm is chosen as 0.2. The P-norm stress constraint is selected as $\sigma^* = 0.65$, and the p-norm parameter is $p = 10$. The initial and optimized designs of L-bracket is plotted in Fig. 12(a) and (b), and the von-Mises stress distribution is shown in Fig. 12(c). Obviously, rounded corners are obtained in the final solution, where the final shape is much smoother than the initial design. The final optimized von-Mises stress is evenly distributed in the design space, where optimized stress distribution is close to a fully stressed design. The evolution of material layout is demonstrated in Fig. 13. As shown in Fig. 13, the boundaries of internal holes move and merge with each other, resulting a non-trivial and optimized shapes. The corresponding evolution of von-Mises distribution is plotted in Fig. 14. The optimization progress takes near 500 iterations to converge as shown in Fig. 15, where the volume fraction of optimized shape is 0.196.

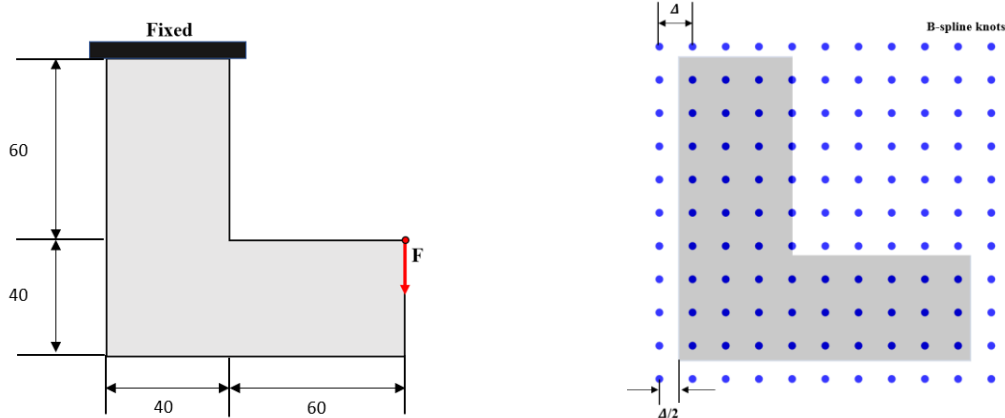


Figure 11. L-bracket design

(a) initial design

(b) optimized design

(c) von Mises stress distribution

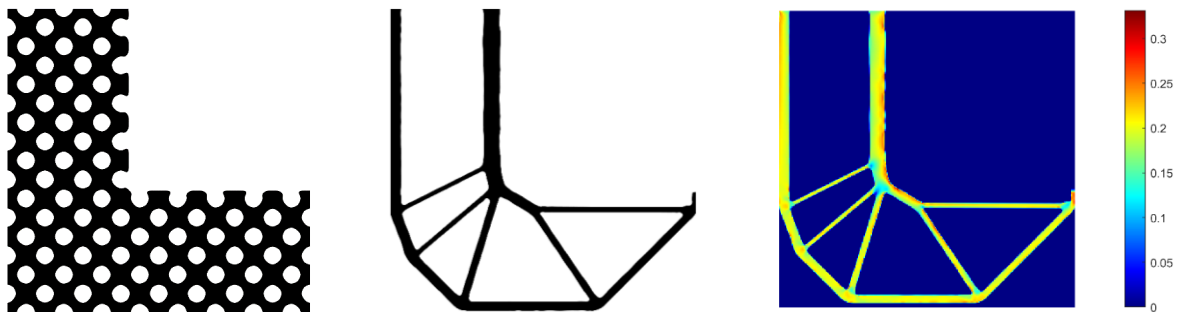


Figure 12. Volume minimization with p-norm stress constraint (a) initial design (b) optimized design (c)

von Mises stress distribution

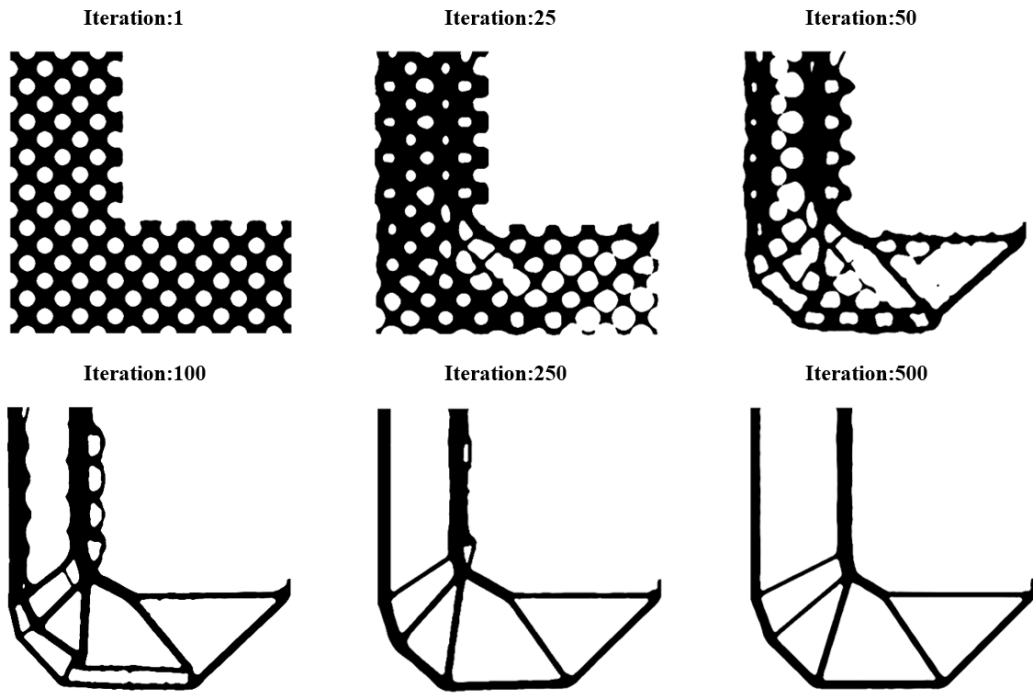


Figure 13. Evolution of material layout during optimization

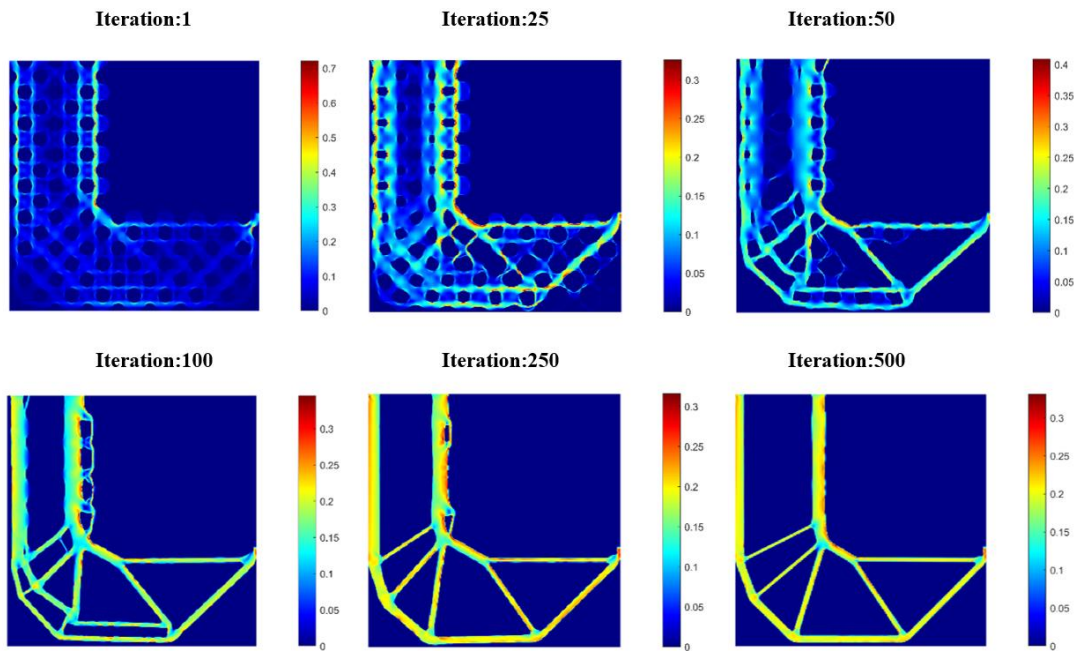


Figure 14. Evolution of von-Mises stress during optimization

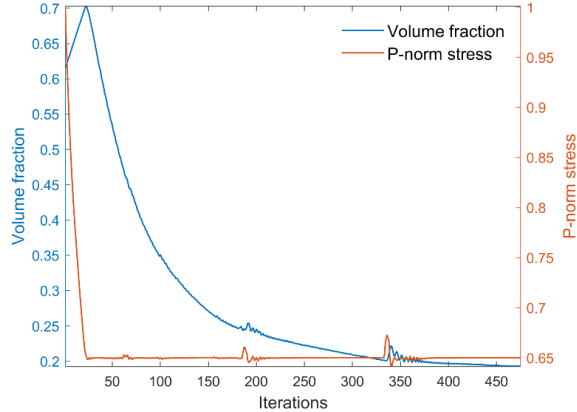


Figure 15. Convergence history

4.2.2 Volume minimization with buckling constraint

In this section, the volume minimization of the L-bracket model with buckling constraint is investigated in the framework of proposed level set method. The finite element discretization and optimization configurations are the same as previous section 4.2.1. a downward concentrated force $F_b = 1 \times 10^{-3}$ is applied on the right upper corner. The buckling constraint μ^* is selected as $\mu^* = 2.5$. Compared with standard density-based method, the local pseudo buckling modes in the low-density regions [33] are not an issue for level set method. The initial design and optimized design are plotted in Fig. 16. In final optimized design (Fig. 16(b)), no slender bars are found, while sharp corner is inevitably generated due to no local stress constraints. Obviously, the optimized structural member in compression becomes wider to against local buckling. The volume fraction reaches 0.307 after near 700 iterations. It is worth to mention that local eigenvalues are very sensitive to boundary move and merge. Jumping phenomenon of eigenvalues may happens during optimization. Therefore, local small fluctuations are found in the convergence history (Fig. 17).

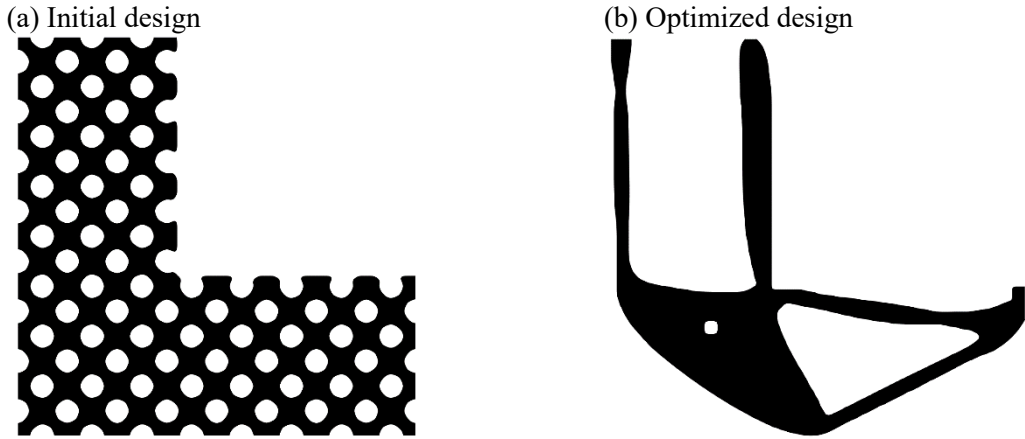


Figure 16. Volume minimization with buckling constraint (a) Initial design (b) Optimized design

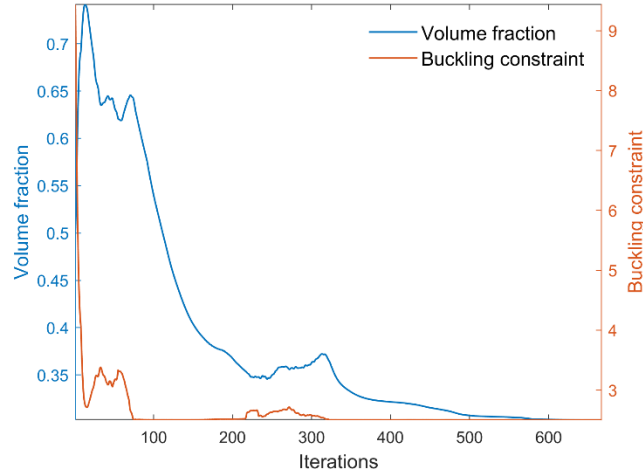


Figure 17. Convergence history

4.2.3 Volume minimization with stress and buckling constraint

In this section, the proposed methodology is applied to solve the problem with stress and buckling constraints. The L-bracket design domain is explored here. The same material properties, discretization method, and optimization configuration are implemented as section 4.2.2 and 4.2.1. Two different loading cases are applied for stress and buckling analysis. For the stress constraint case, the load force is chosen as $F_p = 1$. For the buckling case, the loading is selected as $F_b = 1 \times 10^{-3}$. Similar to section 4.2.2 and 4.2.1, the stress and buckling constraints are set as $\sigma^* = 0.65$ and $\mu^* = 2.5$. Starting with the initial design shown in Fig. 16, the solution for stress and buckling constraints is presented in Fig. 18(a). the correspondent von Mises stress field is presented in Fig. 18(b). As shown in Fig. 18(b), the maximum von Mises stress are evenly distributed nearby the rounded corner. Compared with solution in section 4.2.2, the boundary becomes smoother, and no stress concentration points are found. The minimal volume fraction obtained is 0.509. The optimization converges after near 500 iterations, and the evolution of topology shapes are demonstrated in Fig. 19.

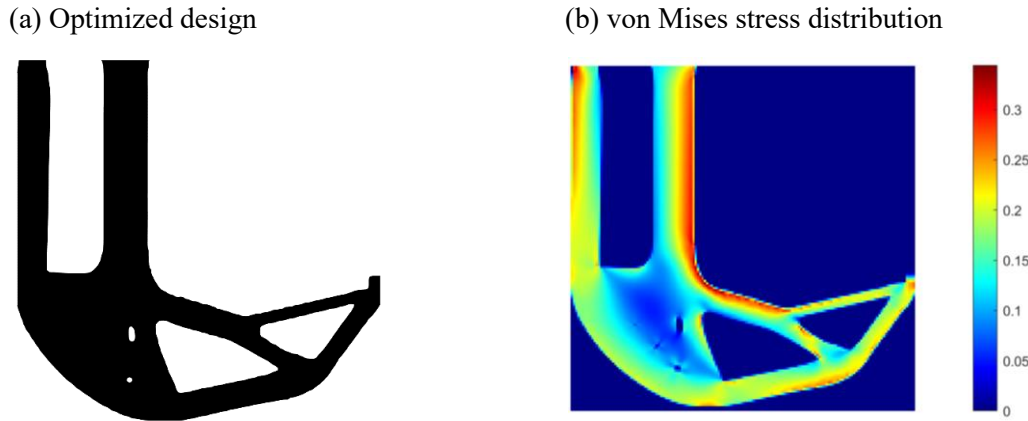


Figure 18. Volume minimization with stress and buckling constraint (a) Optimized design (b) von Mises stress distribution

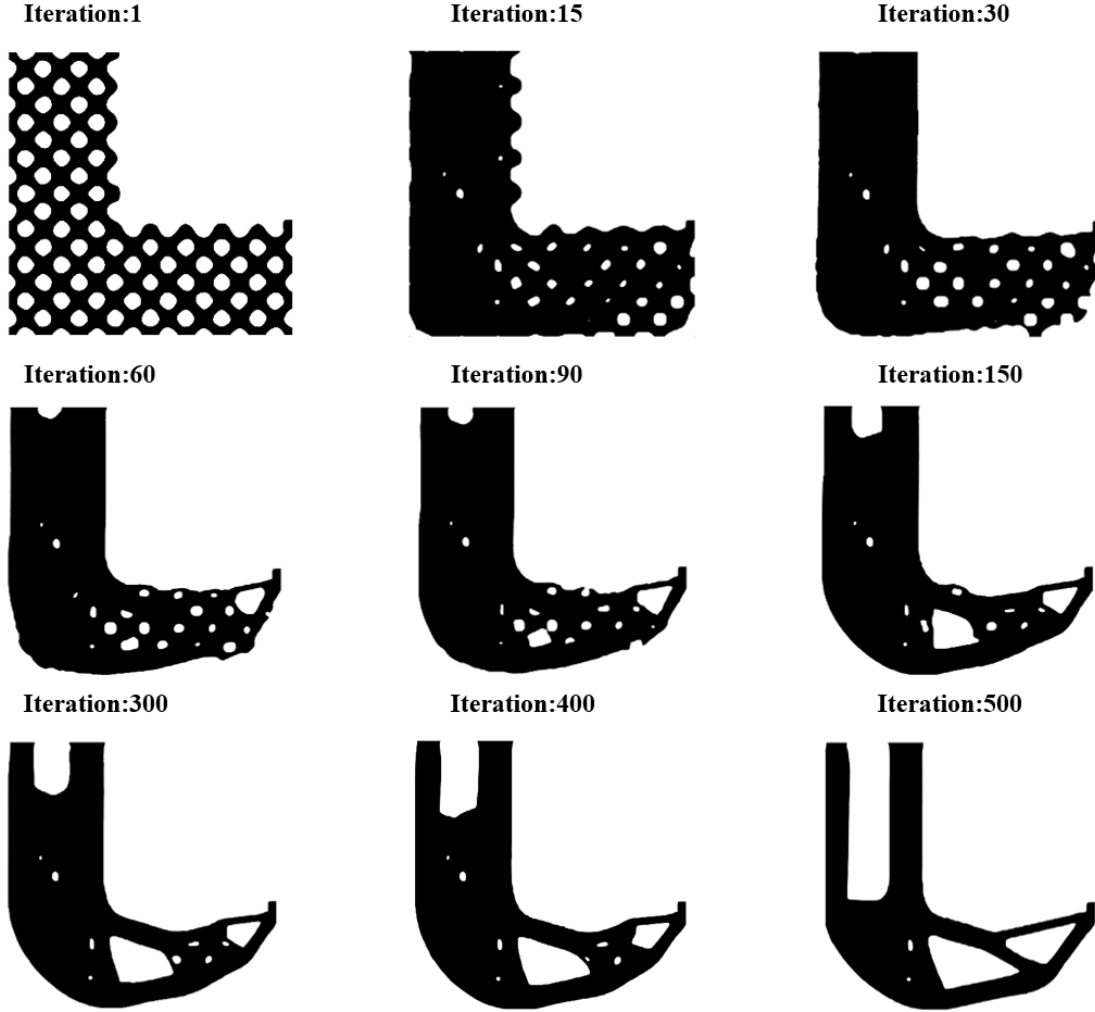


Figure 19. Evolution of material layout during optimization

4. Conclusion

In this paper, a velocity field level set method based on discrete adjoint method is presented, where the velocity field is described in the B-spline space. The analytical sensitivity of presented level set method can be fully computed using the discrete adjoint method, where the mathematical relationship between the level set velocity with discrete adjoint sensitivities are derived and demonstrated in detail. The adjoint equations are derived using the discretized governing equations. The proposed level set sensitivity analysis method does not need any extra smoothing or interpolation typically used in classical level set topology optimization scheme. Note that the proposed sensitivity analysis method is not limited to B-spline space, any other velocity field representation methods [34] are also applied. To demonstrate the effectiveness of proposed sensitivity analysis method, stress and buckling constrained examples are investigated, which are considered to be challenging in level set topology optimization. Meanwhile, multiple constraints are also examined in the framework of proposed level set method.

Reference

- [1] M. P. Bendsøe and O. Sigmund, "Material interpolation schemes in topology optimization," *Archive of applied mechanics*, vol. 69, pp. 635-654, 1999.
- [2] M. Y. Wang, X. Wang, and D. Guo, "A level set method for structural topology optimization," *Computer methods in applied mechanics and engineering*, vol. 192, pp. 227-246, 2003.
- [3] X. Huang and M. Xie, *Evolutionary topology optimization of continuum structures: methods and applications*: John Wiley & Sons, 2010.
- [4] X. Guo, W. Zhang, and W. Zhong, "Doing Topology Optimization Explicitly and Geometrically—A New Moving Morphable Components Based Framework," *Journal of Applied Mechanics*, vol. 81, 2014.
- [5] W. Zhang, J. Chen, X. Zhu, J. Zhou, D. Xue, X. Lei, *et al.*, "Explicit three dimensional topology optimization via Moving Morphable Void (MMV) approach," *Computer Methods in Applied Mechanics and Engineering*, vol. 322, pp. 590-614, 2017/08/01/ 2017.
- [6] W. Zhang, W. Yang, J. Zhou, D. Li, and X. Guo, "Structural topology optimization through explicit boundary evolution," *Journal of Applied Mechanics*, vol. 84, 2017.
- [7] W. Zhang, J. Yuan, J. Zhang, and X. Guo, "A new topology optimization approach based on Moving Morphable Components (MMC) and the ersatz material model," *Structural and Multidisciplinary Optimization*, vol. 53, pp. 1243-1260, 2016/06/01 2016.
- [8] J. A. Norato, B. K. Bell, and D. A. Tortorelli, "A geometry projection method for continuum-based topology optimization with discrete elements," *Computer Methods in Applied Mechanics and Engineering*, vol. 293, pp. 306-327, 2015/08/15/ 2015.
- [9] J. Norato, R. Haber, D. Tortorelli, and M. P. Bendsøe, "A geometry projection method for shape optimization," *International Journal for Numerical Methods in Engineering*, vol. 60, pp. 2289-2312, 2004.
- [10] S. Zhang, A. L. Gain, and J. A. Norato, "Stress-based topology optimization with discrete geometric components," *Computer Methods in Applied Mechanics and Engineering*, vol. 325, pp. 1-21, 2017.
- [11] G. Allaire, F. Jouve, and A.-M. Toader, "Structural optimization using sensitivity analysis and a level-set method," *Journal of computational physics*, vol. 194, pp. 363-393, 2004.
- [12] D. Adalsteinsson and J. A. Sethian, "The fast construction of extension velocities in level set methods," *Journal of Computational Physics*, vol. 148, pp. 2-22, 1999.
- [13] S. Wang and M. Y. Wang, "Radial basis functions and level set method for structural topology optimization," *International journal for numerical methods in engineering*, vol. 65, pp. 2060-2090, 2006.
- [14] Z. Luo, M. Y. Wang, S. Wang, and P. Wei, "A level set-based parameterization method for structural shape and topology optimization," *International Journal for Numerical Methods in Engineering*, vol. 76, pp. 1-26, 2008.
- [15] P. Wei and M. Y. Wang, "Piecewise constant level set method for structural topology optimization," *International Journal for Numerical Methods in Engineering*, vol. 78, pp. 379-402, 2009.
- [16] L. Jiang and S. Chen, "Parametric structural shape & topology optimization with a variational distance-regularized level set method," *Computer Methods in Applied Mechanics and Engineering*, vol. 321, pp. 316-336, 2017.
- [17] Y. Wang, Z. Kang, and P. Liu, "Velocity field level-set method for topological shape optimization using freely distributed design variables," *International Journal for Numerical Methods in Engineering*, vol. 120, pp. 1411-1427, 2019.
- [18] Y. Wang and Z. Kang, "A velocity field level set method for shape and topology optimization," *International Journal for Numerical Methods in Engineering*, vol. 115, pp. 1315-1336, 2018.
- [19] Y. Wang, H. Yang, and Z. Kang, "Velocity field level set method incorporating topological derivatives for topology optimization," *Journal of Applied Mechanics*, vol. 89, p. 061002, 2022.
- [20] N. P. Van Dijk, K. Maute, M. Langelaar, and F. Van Keulen, "Level-set methods for structural topology optimization: a review," *Structural and Multidisciplinary Optimization*, vol. 48, pp. 437-472, 2013.

- [21] S. Kambampati, H. Chung, and H. A. Kim, "A discrete adjoint based level set topology optimization method for stress constraints," *Computer Methods in Applied Mechanics and Engineering*, vol. 377, p. 113563, 2021.
- [22] M. D. Gunzburger, *Perspectives in flow control and optimization*: SIAM, 2002.
- [23] M. P. Bendsoe and O. Sigmund, *Topology optimization: theory, methods, and applications*: Springer Science & Business Media, 2003.
- [24] X. Qian, "Topology optimization in B-spline space," *Computer Methods in Applied Mechanics and Engineering*, vol. 265, pp. 15-35, 2013.
- [25] M. Sarcar, K. M. Rao, and K. L. Narayan, *Computer aided design and manufacturing*: PHI Learning Pvt. Ltd., 2008.
- [26] K. Svanberg, "The method of moving asymptotes—a new method for structural optimization," *International journal for numerical methods in engineering*, vol. 24, pp. 359-373, 1987.
- [27] M. B. Giles, M. C. Duta, J.-D. Muller, and N. A. Pierce, "Algorithm developments for discrete adjoint methods," *AIAA journal*, vol. 41, pp. 198-205, 2003.
- [28] C. Le, J. Norato, T. Bruns, C. Ha, and D. Tortorelli, "Stress-based topology optimization for continua," *Structural and Multidisciplinary Optimization*, vol. 41, pp. 605-620, 2010.
- [29] R. Picelli, S. Townsend, C. Brampton, J. Norato, and H. A. Kim, "Stress-based shape and topology optimization with the level set method," *Computer methods in applied mechanics and engineering*, vol. 329, pp. 1-23, 2018.
- [30] F. Ferrari, O. Sigmund, and J. K. Guest, "Topology optimization with linearized buckling criteria in 250 lines of Matlab," *Structural and Multidisciplinary Optimization*, vol. 63, pp. 3045-3066, 2021.
- [31] F. Ferrari and O. Sigmund, "Towards solving large-scale topology optimization problems with buckling constraints at the cost of linear analyses," *Computer Methods in Applied Mechanics and Engineering*, vol. 363, p. 112911, 2020.
- [32] N. M. Poon and J. R. Martins, "An adaptive approach to constraint aggregation using adjoint sensitivity analysis," *Structural and Multidisciplinary Optimization*, vol. 34, pp. 61-73, 2007.
- [33] X. Gao and H. Ma, "Topology optimization of continuum structures under buckling constraints," *Computers & Structures*, vol. 157, pp. 142-152, 2015.
- [34] Y. Wang and Z. Kang, "MATLAB implementations of velocity field level set method for topology optimization: an 80-line code for 2D and a 100-line code for 3D problems," *Structural and Multidisciplinary Optimization*, vol. 64, pp. 4325-4342, 2021.